Potential energy surface and bound states of the (X4Σ)KRb–K complex

ARTICLE *in* INTERNATIONAL JOURNAL OF QUANTUM CHEMISTRY · JANUARY 2015

Impact Factor: 1.43 · DOI: 10.1002/qua.24759

6 AUTHORS, INCLUDING:

David López-Durán

Spanish National Research Council

32 PUBLICATIONS **285** CITATIONS

SEE PROFILE

Gerardo Delgado-Barrio

Spanish National Research Council

246 PUBLICATIONS **2,961** CITATIONS

SEE PROFILE

Pablo Villarreal

Spanish National Research Council

202 PUBLICATIONS **2,617** CITATIONS

SEE PROFILE

Maria Pilar De Lara-Castells

Spanish National Research Council

72 PUBLICATIONS **726** CITATIONS

SEE PROFILE

Potential Energy Surface and Bound States of the $(X^4\Sigma)$KRb-K Complex

D. López-Durán,*,†[a] N. F. Aguirre,‡[a] G. Delgado-Barrio,[a] P. Villarreal,[a] F. A. Gianturco,[b] and M. P. de Lara-Castells[a]

We present in this work a potential energy surface of the $(X^4\Sigma)$KRb-K complex for which high level *ab initio* calculations have been carried out at the RCCSD(T) level of theory, using ECP10MDF/ECP28MDF effective core potentials and basis sets for K/Rb, respectively, with the dimer at its lowest triplet $^3\Sigma$ state and fixed to the equilibrium distance. The interaction is shown to be very anisotropic, with one clear minimum at a T-type geometry of the complex. The depth of the well is found to be 767.7 cm^{-1} located at R=4.60 Å, θ=105° in Jacobi coordinates from the center of mass of the diatomic partner. A variational (VAR) procedure and the Diffusion Monte Carlo technique have been applied to explore the bound states of the aggregate. Both descriptions provide similar features for the vibrational, nonrotating, ground-state, with an energy of ~ -737.8 cm^{-1} and the maximum of the wavefunction peaked above the well of the surface. Excited states are also reported using the VAR treatment and angular and/or radial excitations are identified among the lower-lying vibrational states. These results should already provide an initial step toward a more comprehensive study of the collisions at ultralow temperatures of K+KRb, important process in the field of ultracold molecular chemistry. © 2014 Wiley Periodicals, Inc.

DOI: 10.1002/qua.24759

Introduction

Cold molecules are currently a very active field of research. Although atoms are perhaps easier to study, molecules give rise to new fascinating and surprising effects, which in some cases are counterintuitive; especially, when the temperatures are of the order of the millionth of K. At very low energies, the de Broglie wavelengths of the molecules are larger than their own size and quantum mechanics rules the scattering process. High precision measurements,[1,2] quantum information,[3] ultracold chemistry,[4] or quantum many-body systems,[5,6] are some examples of application in yet insufficiently explored topics.

A big effort in the production of ultracold alkali-metal dimers has been made and the most common tool to provide weakly bound KRb molecules is the Feshbach spectroscopy.[7–10] The creation and characterization of weakly bound heteronuclear KRb Feshbach molecules[11,12] followed by coherent transfer to low-energy states through stimulated Raman adiabatic passage (STIRAP,[13–15]) gave rise to ultracold dense gases of KRb in the rovibrational ground-state of either the triplet or the singlet electronic ground-state.[16] Other molecules like ultracold Rb_2 in the lowest rovibrational state of the lowest triplet state[17] and ultracold Cs_2 in its ground rovibronic state[18] have also been trapped. Precise control of the molecular electronic ($^1\Sigma$), vibrational, rotational,[19] and hyperfine[20] degrees of freedom were achieved later on. The experiments show evidence of undesired exothermic atom-exchange chemical reactions for species in their absolute ground-state, KRb+KRb $\rightarrow K_2+Rb_2$, and the effect of the initial state on the final result was reported. If molecules are prepared in a single state the reaction rate is strongly suppressed by the Pauli principle and collisions are expected to proceed predominantly *via* tunneling through the p-wave barrier. However, if two different internal states are considered the reaction rates are enhanced by a factor of 10–100 as a result of the barrierless s-wave scattering.[21] In the presence of an electric field, the thermodynamics of the dipolar gas makes it possible to direct observe the spatial anisotropy of the dipolar interaction and its influence on the loss rates.[22] Creating a long-lived ensemble of ultracold polar molecules may require restriction to a two–dimensional (2D) trap geometry to suppress the attractive, "head-to-tail", dipolar interactions[22]; a result achieved through the convenient orientation of the dipoles, "side-by-side," along the tight confinement direction in a quasi-2D geometry of an optical lattice and resulting in the decreasing of the bimolecular chemical reaction rate by nearly two orders of

[a] *D. López-Durán, N. F. Aguirre, G. Delgado-Barrio, P. Villarreal, M. P. de Lara-Castells*
Instituto de Física Fundamental, IFF-CSIC, Serrano 123, 28006 Madrid, Spain
E-mail: d.lopez.duran@csic.es
[b] *F. A. Gianturco*
Institute of Ion Physics, Innsbruck University, Technikerstr. 25, 6020 Innsbruck, Austria and Scuola Normale Superiore, Piazza dei Cavalieri, 50125 Pisa, Italy

Contract grant sponsor: MICINN; contract grant numbers: FIS2010-18132 and FIS2011–29596-C02-01.
Contract grant sponsor: Spanish programs JAE-PREDOC (N. F. A) and JAE-DOC (D. L.-D.); contract grant number: E-28-2009-0448699.
Contract grant sponsor: PRIN Project 2009 (F. A. G.).

†*Present address*: Departamento de Química Analítica, Química Física e Ingeniería Química, Universidad de Alcalá, 28871 Alcalá de Henares, Madrid, Spain

‡*Present address*: Departamento de Química, Universidad Autónoma de Madrid, 28049 Madrid, Spain

magnitude.[23] The measurement of the anisotropic polarizability of the dimer[24] is another step in the production of new molecule-based quantum systems, precise spectroscopic measurements, coherent manipulations of the species, and probing novel quantum many-body states of polar molecules. Atom-diatom collisions may also take place in the experiment, specifically during the initial part, the Feshbach association. Loss of KRb dimers due to background K atoms is expected because of the exothermic chemical reaction $K+KRb \rightarrow K_2+Rb$, while the endothermic process $Rb+KRb \rightarrow K+Rb_2$ with remaining Rb particles is forbidden.[21] The lifetime of the diatom is also limited by inelastic collisions as well, and the effect of the potassium on the lifetime of KRb has dramatic consequences (see Figure 13 of Ref. [25]).

To study K+KRb collisions a realistic knowledge of the potential energy surface (PES) of the complex is a prerequisite and we have not found in the literature any detailed description of this interaction. Therefore, we present in this article the first high level *ab initio* PES in which the KRb is in the lowest triplet $^3\Sigma$ state and the KRb-K in the $^4\Sigma$ one, as well as a study of its bound and excited states through a variational (VAR) procedure and a Diffusion Monte Carlo (DMC) technique. Since our interest is focused on rotational cooling collisions, we have kept the dimer fixed at its equilibrium geometry. Also, some additional calculations have been carried out by relaxing that constraint. Previous studies on the K_2Rb aggregate have been already reported, in which high-level electronic structure calculations of all the heteronuclear alkali-metal species were performed, exploring also the energetics of the reactions involved.[26,27] Two relevant symmetries are found for KRb_2 and K_2Rb: C_{2v} and C_s. Both works agree in the most stable symmetry for KRb_2, C_{2v}; but disagree for K_2Rb: C_s in Ref. [26] and C_{2v} in Ref. [27]. Such a discrepancy can be explained in terms of the more accurate level of theory used in Ref. [26] (multireference coupled-cluster) as compared to Ref. [27] (single-reference coupled-cluster). A more detailed description seems to reflect Jahn–Teller-like distortions for K_2Rb in its doublet state, with the ensuing change from C_{2v} to C_s[26] (heteronuclear trimers in doublet states do not show true Jahn–Teller effects). The K_2Rb_2 aggregate at its ground-state presents two stable planar structures for D_{2h} and C_s symmetry.[27] Trimer formation reactions are always forbidden for low-lying singlet states of the dimers (but can be formed from dimers in triplet states or excited vibrational states, for instance[26]) and in both works the atom exchange between dimers of KRb to form homonuclear diatoms is allowed. Homonuclear trimers of alkali-metal atoms have also been studied: the lowest quartet electronic states of Na_3,[28] K_3,[29] and Li_3,[30] for example. The configuration for the minimum in all the cases corresponds to a D_{3h} point group as there are no Jahn–Teller distortions for being quartet states. A reduction from the dimer to the trimer equilibrium distance is always obtained, ranging in the 10–25%. Bound states calculations of quartet states of Na_3[28,31,32] show a good agreement between the experimental and the theoretical spectra and the calculated vibrational frequencies of the two normal modes are ν_1=37.1 cm^{-1} and ν_2=40.8, 44.7 cm^{-1} for Ref. [28] and ν_1=38 cm^{-1} and ν_2=41 cm^{-1} for Ref. [31]. In the region of high-lying states two special cases are found, which result to be also present in Ar_3: "horseshoe" and "linear symmetric stretch" states; the former being characterized by a motion in which the molecule passes from one equilateral triangle geometry to another equivalent geometry (one atom moves between the other two and the outer atoms move apart to make room for it).[32] The study of the $Li+Li_2$ collisions at its quartet states showed that for low initial vibrational states the quenching rates are not suppressed for fermionic atoms[30,33]; while for $(^2S)K+(^3\Sigma)K_2$ the vibrational quenching is much faster than elastic scattering in the ultralow-temperature regime.[29] The $Na+Na_2$ collision at its quartet state illustrates the need of an accurate PES: the rate coefficients for the vibrational relaxation $v=1\rightarrow0$ differ one order of magnitude depending on whether the nonadditive terms are included or not.[34] A realistic PES is a very sensitive part in the study of collisions at low and ultralow temperatures and the results obtained with any theoretical method are strongly influenced by its shape.[35,36] Our aim in this article is to provide a reliable description of the full electronic potential energy as a first step in the research of the KRb-K complexes.

The article is organized as follows. A full description of the PES can be found in section 2. Section 3 describes the theory of both computational methodologies we have used here to search for the bound states of the aggregate, while in section 4 their main features are shown. Our present conclusions constitute section 5.

The Interaction Potential

Ab initio electronic structure calculations

All *ab initio* calculations have been carried out with the MOLPRO 2006.1 package,[37] using the spin restricted single and double excitations coupled cluster method with perturbative triples [RCCSD(T)], correlating only the valence electrons, and including the BSSE correction.[38] In the case of the dimer we have treated the $1s^22s^22p^6/1s^22s^22p^63s^23p^63d^{10}$ electrons as core and the $3s^23p^64s^1/4s^24p^65s^1$ electrons as valence for K/Rb, respectively. The $(^3\Sigma)$KRb potential curve has been generated using the ECP10MDF / ECP28MDF effective core potentials[39] (ECP) for the core electrons, while for the valence ones four basis sets has been tested:

1. The ECP10MDF/ECP28MDF[39] defined as $(11s,11p,5d,3f)$ / $(13s,10p,5d,3f,1g)$, with 90/98 primitive Gaussian functions per atom.
2. An enlarged version of the same set in which even tempered diffuse functions $(1s,1p,1d,1f,1g)$ for both K and Rb have been added together with a g function in the K case (0.61219)—$(12s,12p,6d,4f,2g)/(14s,11p,6d,4f,2g)$ -, with a total of 124/123 primitive Gaussian functions per atom, denoted as "ECP10MDF-enl/ECP28MDF-enl."
3. The def2-TVZPP/def2-QVZPP[40] defined as $(17s,11p,3d)$ / $(8s,8p,5d,3f)$, with 65/78 primitive Gaussian functions per atom.

Table 1. Equilibrium distance, r_{eq} (in Å), and well depth, D_e (in cm^{-1}), calculated with different basis set for ($X^3\Sigma$)KRb.

K basis set	Rb basis set	r_{eq}	D_e
ECP10MDF	ECP28MDF	5.980	220.95
ECP10MDF-enl	ECP28MDF-enl	5.952	232.86
def2-TZVPP	def2-QZVPP	6.036	221.91
def2-QZVPP	def2-QZVPP	6.008	213.49
Klempt *et al.*, Ref. [9]		–	240.024
Pashov *et al.*, Ref. [41]		5.9029(1)	249.031(10)
Rousseau *et al.*, Ref. [42]		5.87	238.3556
Park *et al.*, Ref. [43]		5.94	244.5150
Kotochigova *et al.*, Ref. [44]		5.92	299.1064
Soldán *et al.*, Ref. [45]		5.945	232.72
Soldán, Ref. [46]		5.89	237

Earlier experimental (Klempt and Pashov) and theoretical (Rousseau, Park, Kotochigova, and Soldán) reported values of these magnitudes are also included.

4. The def2-QZVPP/def2-QZVPP[40] in which the new basis set for K is $(24s, 18p, 4d, 3f)$, with 119 primitive Gaussian functions per atom.

In Table 1, we show our values for the equilibrium distance r_{eq} and the well depth D_e, together with other available values. At first sight r_{eq} varies between 5.8 and 6.0 Å and D_e between 200 and 300 cm^{-1}, approximately. Our calculations of r_{eq} are slightly above of the experimental data of Pashov *et al.*, Ref. [41], but also close to other values found in the literature. With respect to D_e all the previous works give values above ours, especially in the case of Kotochigova *et al.*[44] (the results of Refs. [42–44] are gathered in Ref. [47]). The best result might have come from using the basis sets ECP10MDF-enl/ECP28MDF-enl, but it has been ruled out due to the large time needed in performing those calculations. ECP10MDF/ECP28MDF and def2-TZVPP/def2-QZVPP are much more feasible, selecting finally the former set (r_{eq}=5.980 Å, D_e=220.95 cm^{-1}), which kept the computational effort within acceptable limits.

To describe the PES of the ($^4\Sigma$)KRb-K complex we have used Jacobi coordinates (r, R, θ). r is the modulus of $\vec{r}$, the stretching motion vector of the dimer, pointing from K to Rb, R is that of $\vec{R}$, the vector joining the center of mass of the KRb with the K atom, and θ is the angle between $\vec{r}$ and $\vec{R}$. A total number of about 1650 points have been calculated, with the angle varying from 0° to 180°, incremented by 7.5°, and adding several extra orientations for a better description of the PES; distances were extended out to 29 Å. The basis set and core for the K atom in the trimer that does not belong to the dimer has been the same as in the KRb case, ECP10MDF.[39]

Analytical representation of the potential energy surface

To obtain the analytical PES of the ($^4\Sigma$)KRb-K trimer we have followed a two-steps plan. First, we have fitted the *ab initio* points at each angle to a Morse function:

$$V(R,\theta)=D_0\{\exp(-2\alpha(R-R_\varepsilon))-2\exp(-\alpha(R-R_\varepsilon))\}. \quad (1)$$

The interpolation has yielded a root mean square (RMS) of the *ab initio* points around 3 cm^{-1}, except in the range 110°–140°, where this RMS is 12 cm^{-1}. We have excluded the angles θ=120° and 123.75° because they cause a higher global error in the fitting. As we have now a 2D representation of the $(D_0, \alpha, R_\varepsilon)$ parameters an interpolation by cubic splines has been carried out in the second step. The final test was to compare the fitted values with the raw points including only those for which the total interaction is lower than 800 cm^{-1}, obtaining a RMS of 0.46 cm^{-1} and which shows the excellent quality of the fitting, Figure 1.

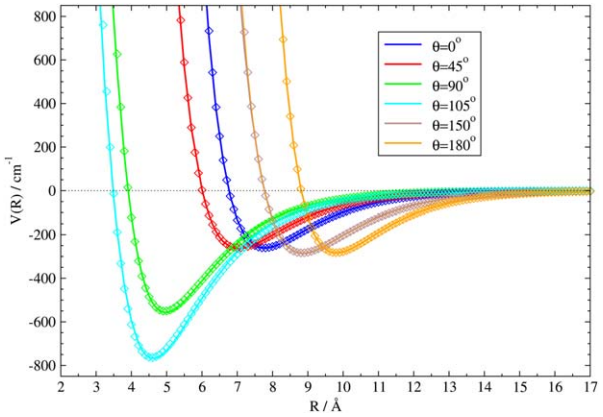

Figure 1. Morse fitting (line) to the *ab initio* points (diamonds) at some orientations for the ($X^4\Sigma$)KRb-K interaction. [Color figure can be viewed in the online issue, which is available at wileyonlinelibrary.com.]

Figure 2 shows the 2D contour plot of the ($X^4\Sigma$)KRb-K PES in the *XY* plane (strictly, the state of the complex can be referred to as the $X^4\Sigma$ state only at linear geometries). By fixing the KRb distance to the equilibrium value, the minimum is located at a configuration of C_s symmetry with R = 4.60 Å, θ=105°, and an interaction energy V_{min}=–767.7 cm^{-1} (R = 4.59 Å, θ=106.46°, and V_{min}=–765.4 cm^{-1} after the fitting). As recently reported by Soldán,[46] the global minimum turns out to be of C_{2v} symmetry, with R = 5.12 Å, θ = 122°, and V_{min}=–1246 cm^{-1}. Moreover, the KRb distance in the bare dimer shortened by about 0.8 Å in the trimer.[46] As aforementioned, we are aimed to study rotational cooling

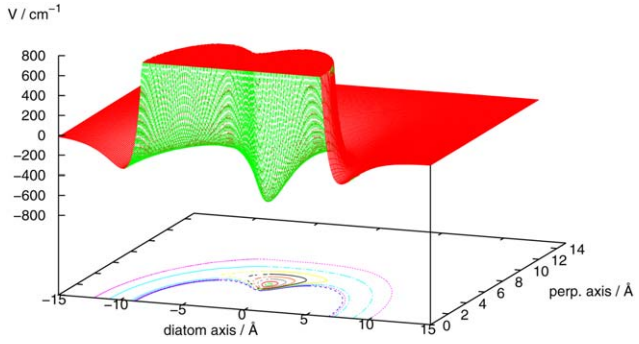

Figure 2. PES in the *XY* plane, with X=$R\cos\theta$ and Y=$R\sin\theta$. Isolines are plotted from −700 to 0 cm^{-1} with an interval of 100 cm^{-1}, as well as the corresponding to −750 cm^{-1} (to render the plot clearer we have included a cut at V = 800 cm^{-1}; which is not enforced in the real surface). [Color figure can be viewed in the online issue, which is available at wileyonlinelibrary.com.]

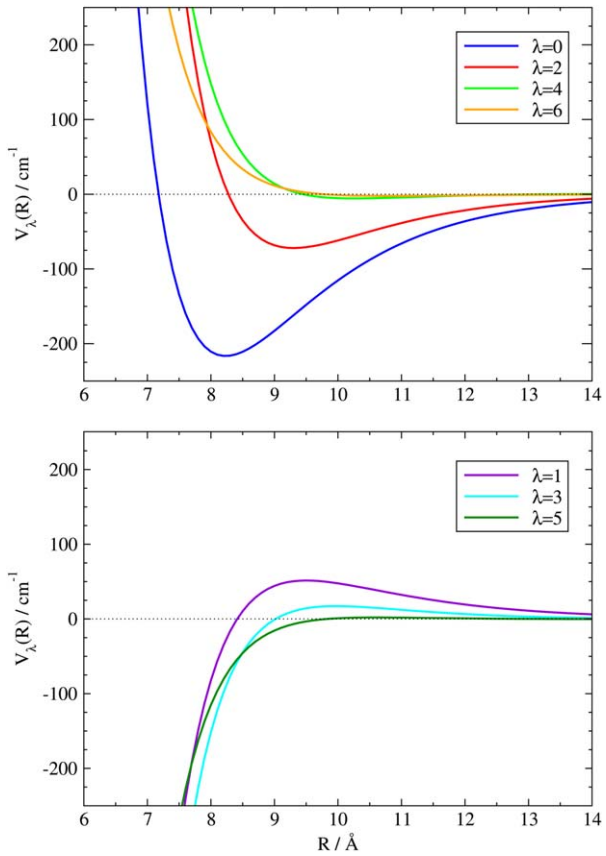

Figure 3. Seven first $V_\lambda(R)$ coefficients for the $(X^4\Sigma)$KRb-K interaction. [Color figure can be viewed in the online issue, which is available at wileyonlinelibrary.com.]

collisions so that the KRb distance has been fixed to the equilibrium value. For the sake of completeness, we have also optimized the KRb elongation in the trimer after fixing the Jacobi θ angle to the equilibrium orientation of 105°. The bare dimer KRb distance (5.98 Å) becomes reduced to 5.35 Å in the trimer, with $V_{\min}$ being lowered from -767.7 cm^{-1} to -864.0 cm^{-1}. Both the reduction of the repulsive Hartree–Fock contribution and the increase of the attractive correlation counterpart have been found to be responsible of the total interaction energy lowering on decreasing the KRb distance.

The V_λ coefficients in the expansion of the potential are:

$$V(R,\theta)=\sum_{\lambda=0}^{\infty} V_\lambda(R)P_\lambda(\cos\theta). \quad (2)$$

If we multiply by $P_{\lambda'}(\cos\theta)$ and integrate between -1 and 1 the expression of each $V_\lambda(R)$ is obtained:

$$V_\lambda(R)=\frac{2\lambda+1}{2}\int_{-1}^{1} P_\lambda(\cos\theta)V(R,\theta)d\cos\theta. \quad (3)$$

V_0 to V_6 are presented in Figure 3 and the dominance of the first four radial coefficients is clearly seen. The *ab initio* data and the PES are available on request from the authors.

Asymptotic correction

Naturally, the Morse functional used to fit the *ab initio* data entails an exponential decay at the long-range region instead of the $\sim-\frac{1}{R^6}$ asymptotic behavior arising from the dispersion energy contribution. At a variance with the calculation of the lowest-lying bound states, collisional dynamical calculations necessitate potentials with the proper long-range tail. For this purpose, the Morse potential has been asymptotically corrected following a similar scheme to that devised by Grüning *et al.*[48] for the exchange-correlation potentials defined within the density-functional-theory framework. This way, the bulk region of the Morse potential is left unperturbed. Specifically, the proposed functional form for the aymptotically corrected potential is

$$V^{\text{Morse-AC}}(R;\theta)=(1-f(R;\theta))V^{\text{Morse}}(R;\theta)+f(R;\theta)V^{\text{AC}}(R), \quad (4)$$

where $V^{\text{AC}}(R)$ is given by

$$V^{\text{AC}}(R)=-\frac{C_6}{R^6}-\frac{C_8}{R^8} \quad (5)$$

and $f(R;\theta)$ is the same function used by Grüning *et al.*:

$$f(R;\theta)=\frac{1}{1+\exp\{-\alpha_{\text{AC}}(R-R_{\text{AC}}(\theta))\}}, \quad (6)$$

which becomes unity in the long-range region and, choosing properly the parameters α_{AC} and R_{AC}, vanishes in the bulk potential region, in which the Morse functional performs remarkably well (see above). For example, $f(R;\theta)=\frac{1}{2}$ if $R=R_{\text{AC}}$. Conversely, the parameter α_{AC} accounts for the switching rate between the Morse and the asymptotic functional forms. To extract the orientational-independent values of the C_6 and C_8 coefficients, we have fitted the correlation contributions to the interaction energy at distances where the Hartree–Fock component is virtually zero. Since the Hartree–Fock method is obviously dispersionless, our choice ensures that the fitting is being done to the purely dispersion energy contribution. Next, the α_{AC} and R_{AC} parameters were fitted to the CCSD(T) interaction energies by fixing the atom-molecule orientation to that of the global minimum (i.e., $\theta=105°$). This procedure provided the values of $\alpha_{\text{AC}}=0.56\,a_0^{-1}$ and $R_{\text{AC}}=20.21\,a_0$. The optimized distance coincided almost perfectly with the point where the $V_{\text{AC}}(R)$ and $V_{\text{Morse}}(R)$ potentials come together, as expected. The same holds true for the other angular orientations. We also tested that the fitted α_{AC} value at $\theta=105°$ works also very well at any angle so that it was fixed. Finally, the small roughness of the R_{AC} dependence on θ (relecting numerical inaccuracies) was smoothed out *via* fitting to the following functional form with $y=\frac{\theta}{\pi}$ as the argument:

$$R_{\text{AC}}(y)=a_{\text{R}}+b_{\text{R}}\cos\pi t_{\text{R}}(r)+c_{\text{R}}\cos 2\pi t_{\text{R}}(r), \quad (7)$$

with

$$t_{\text{R}}(R)=y^{\gamma_{\text{R}}}+\tau_{\text{R}}\sin 2\pi y^{\gamma_{\text{R}}}. \quad (8)$$

Figure 4 compares the total potential at $\theta=105°$ with and without the asymptotic correction while Table 2 lists the

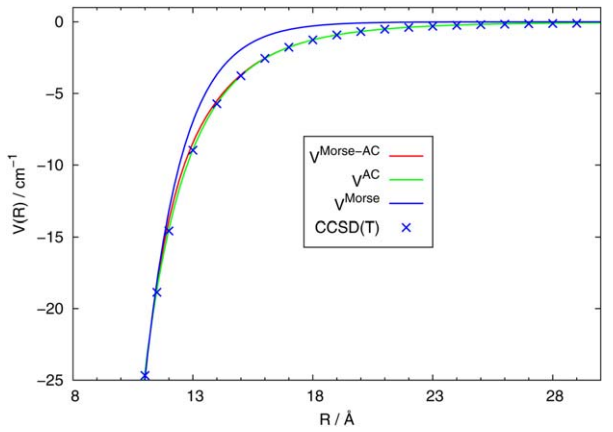

Figure 4. Comparison between the potentials at $\theta=105^{\circ}$ obtained with and without including the asymptotic correction. [Color figure can be viewed in the online issue, which is available at wileyonlinelibrary.com.]

numerical values of the different parameters. For atom-diatom distances larger than R_{AC}, the correction lowers the average unsigned relative error with respect to the *ab initio* data by more than a factor of three, while the counterpart in the bulk potential region ($R \leq R_{AC}$) is kept nearly unperturbed (to within 0.08 %). It is stressed that the lowest-energy bound state energies were left almost unchanged (to within 2 %). To check the quality of the dispersion part, we have calculated also the corresponding coefficients C_6 and C_8 for K_2 and KRb. For K_2, the coefficients, $3.942 \times 10^3\ E_h\ a_0^6$ and $3.9 \times 10^5\ E_h\ a_0^8$, agree very well to the published values of $3.897 \times 10^3\ E_h\ a_0^6$ and $4.2 \times 10^5\ E_h\ a_0^8$ from Refs. [49,50]. The same holds true for KRb, with coefficients of $4.378 \times 10^3\ E_h\ a_0^6$, and $4.3 \times 10^5\ E_h\ a_0^8$; to compare with $4.274 \times 10^3\ E_h\ a_0^6$ and $4.9 \times 10^5\ E_h\ a_0^8$ from Refs. [50,51].

Bound States Calculation

Variational method

The Hamiltonian of a K atom bound to a KRb molecule considered as a pseudo-$^1\Sigma$ partner (i.e., the spin effects are ignored) can be written in Jacobi coordinates in the following way[52,53]:

$$H=\frac{\vec{j}^{\,2}}{2m_{KRb}r_{eq}^2}-\frac{\hbar^2}{2m}\frac{\partial^2}{\partial R^2}+\frac{\vec{l}^{\,2}}{2mR^2}+V(R,\theta), \tag{9}$$

where we have assumed that the diatom is a rigid rotor with its intramolecular distance fixed at the equilibrium value r_{eq}, $m_{KRb}=m_K+m_{Rb}$, with m_K/m_{Rb} being the mass of the K/Rb atom, and $\frac{1}{m}=\frac{1}{m_{KRb}}+\frac{1}{m_K}$. $\vec{r}$ is the vector related to the vibration of the KRb subunit and $\vec{R}=(R,\theta)$ describes the movement of the potassium with respect to the dimer. $\vec{j}$ and $\vec{l}$ are the angular momentum operators associated with $\vec{r}$ and $\vec{R}$, respectively, whose coupling leads to the total angular momentum $\vec{J}=\vec{j}+\vec{l}$. More correctly, the total diatomic angular momentum $\vec{j}$ should be replaced in Eq. (9) by the nuclear diatomic rotational angular momentum which in the case of a $^3\Sigma$ state of an alkali dimer corresponds[54] to a Hund's case (b)[55,56]: $\vec{N}=\vec{j}-\vec{S}$, with $\vec{S}$ the electronic spin operator. In addition, spin coupling effects, like spin–spin and spin-rotation, should be incorporated in a more complete Hamiltonian; but given the smallness of these coupling terms no major effect on the final interaction potential is expected by their inclusion. $V(R,\theta)$ represents the KRb-K PES.

We now consider a body-fixed (BF) frame with the Z^{BF} axis parallel to $\hat{R}$, which is the unitary vector of $\vec{R}$, and basis functions of the form:

$$\Psi_{nj\Omega}^{JM}(\vec{R},\hat{r})=f_n(R)W_{j\Omega}^{JM}(\hat{R},\hat{r}). \tag{10}$$

$f_n(R)$ are radial functions associated with the KRb-K stretching motion, numerically obtained when searching for the ground-state energy level, E_n, of a set of Schrödinger equations at different orientations $\{\theta_n\}_{n=1,\ldots,N}$[57]:

$$\left\{-\frac{\hbar^2}{2\mu}\frac{\partial}{\partial R^2}+V(R,\theta_n)\right\}\varphi(R;\theta_n)=E_n\varphi(R;\theta_n). \tag{11}$$

A further orthogonalization of the eigenfunctions $\varphi(R;\theta_n)$ through a Schmidt procedure leads to an orthonormal set $\{f_n(R)\}_{n=1,\ldots,N}$.

$W_{j\Omega}^{JM}$ are the angular wavefunctions which depend on the orientation $\hat{R}\equiv(\theta_R,\phi_R)$ with respect to a space-fixed reference system and on the orientation $\hat{r}\equiv(\theta,\phi)$ in the BF frame. They can be expressed as[58]:

$$W_{j\Omega}^{JM}(\hat{R},\hat{r})=\sqrt{\frac{2J+1}{4\pi}}D_{M\Omega}^{J*}(\phi_R,\theta_R,0)Y_{j\Omega}(\theta,\phi), \tag{12}$$

being $D_{M\Omega}^{J}$ the Wigner rotation matrices and $Y_{j\Omega}$ the spherical harmonics. J, M, and Ω are the quantum number associated with the total angular momentum $\vec{J}$, and with the projections of $\vec{J}$ on Z^{SF} and Z^{BF}, respectively.

The relevant symmetry operator of the system is the total inversion ε^*, whose action on the angular wavefunctions is:

$$\varepsilon^* W_{j\Omega}^{JM}=(-1)^j W_{j,-\Omega}^{JM}. \tag{13}$$

Therefore, a symmetry-adapted basis set is defined as

$$\Psi_{nj\Omega}^{JM\epsilon}(\vec{R},\hat{r})=f_n(R)\Theta_{j\Omega}^{JM\epsilon}(\hat{R},\hat{r}), \tag{14}$$

which is eigenfunction of ε^* with eigenvalue ϵ, and where

$$\Theta_{j\Omega}^{JM\epsilon}=\frac{1}{\sqrt{2(1+\delta_{\Omega 0})}}\left\{W_{j\Omega}^{JM}+\epsilon W_{j,-\Omega}^{JM}\right\}. \tag{15}$$

Evaluating the radial functions through quadratures and expanding the KRb-K interaction into Legendre polynomials all

Table 2. Parameters for the asymptotic correction.

α_{AC} (a_0^{-1})	0.56
a_R (a_0)	24.79
b_R (a_0)	−4.85
c_R (a_0)	6.97
γ_R	1.02
τ_R	−0.14
C_6 ($E_h\ a_0^6$)	8.857×10^3
C_8 ($E_h\ a_0^8$)	4.9×10^5

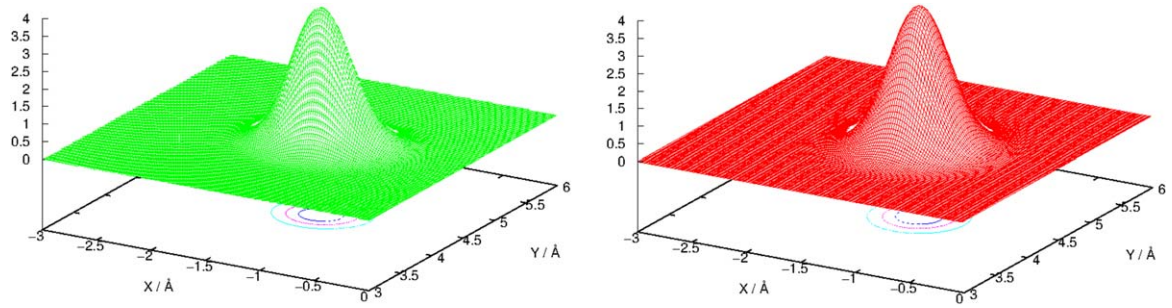

Figure 5. VAR (left) and DMC (right) wavefunctions for the ground vibrational states from the present calculations. [Color figure can be viewed in the online issue, which is available at wileyonlinelibrary.com.]

the matrix elements of the Hamiltonian in Eq. (9) become analytical[52,53] and the eigenvalue problem is solved using standard routines.[59,60]

Diffusion Monte Carlo approach

The DMC method has been discussed several times before and we will only summarize here its main features (we suggest Refs. [61–67] for further details). Taking into account that the dimer rotation is for the moment disregarded, the Hamiltonian of a KRb-K complex can be expressed as:

$$H=-\frac{\hbar^2}{2m_{\mathrm{KRb}}}\nabla^2_{\mathrm{KRb}}-\frac{\hbar^2}{2m_{\mathrm{K}}}\nabla^2_{\mathrm{K}}+V(\vec{R}). \tag{16}$$

$\vec{R}\equiv\{\vec{R}_{\mathrm{KRb}},\vec{R}_{\mathrm{K}}\}$ and collects the cartesian coordinates of the diatom and the K atom, with the spatial derivatives ∇_i referred to them. $V(\vec{R})$ is the diatom-potassium interaction.

From the time-dependent Schrödinger equation with imaginary time $\tau\equiv-\frac{it}{\hbar}$ and the distribution function $f(\vec{R},\tau)\equiv\Psi_{\mathrm{T}}(\vec{R})\Psi(\vec{R},\tau)$ we arrive after a little algebra to the following expression:

$$-\frac{\partial f(\vec{R},\tau)}{\partial\tau}=-\sum_{i=\mathrm{KRb,K}}\left(D_i\nabla_i^2 f(\vec{R},\tau)+D_i\nabla_i\cdot[\vec{F}(\vec{R})\cdot f(\vec{R},\tau)]\right)+[E_{\mathrm{L}}(\vec{R})-E_{\mathrm{T}}]f(\vec{R},\tau). \tag{17}$$

$\Psi_{\mathrm{T}}(\vec{R})$ is an analytical trial function which approximates at best the true ground-state wavefunction, $D_i\equiv\frac{\hbar^2}{2m_i}$ takes the form of a diffusion coefficient, $\vec{F}(\vec{R})$ is the quantum force, $E_{\mathrm{L}}(\vec{R})$ is the local energy, and E_{T} is the reference energy. The DMC procedure is based on the short-time approximation[68] and the Schrödinger equation is solved iteratively:

$$\Psi(\vec{R}',\tau_{k+1})=\int G(\vec{R}'\leftarrow\vec{R},\triangle\tau)\Psi(\vec{R},\tau_k)d\vec{R}, \tag{18}$$

where $\triangle\tau=\tau_{k+1}-\tau_k$ is now the discretized time step and $G(\vec{R}'\leftarrow\vec{R},\triangle\tau)$ the Green's function:

$$G(\vec{R}'\leftarrow\vec{R},\triangle\tau)=\langle\vec{R}'|\exp\left(-\triangle\tau(H-E_{\mathrm{T}})\right)|\vec{R}\rangle. \tag{19}$$

$G(\vec{R}'\leftarrow\vec{R},\triangle\tau)$ can be interpreted as the "transition" probability to move from $\vec{R}$ to a new position $\vec{R}'$ in the time step $\triangle\tau$.

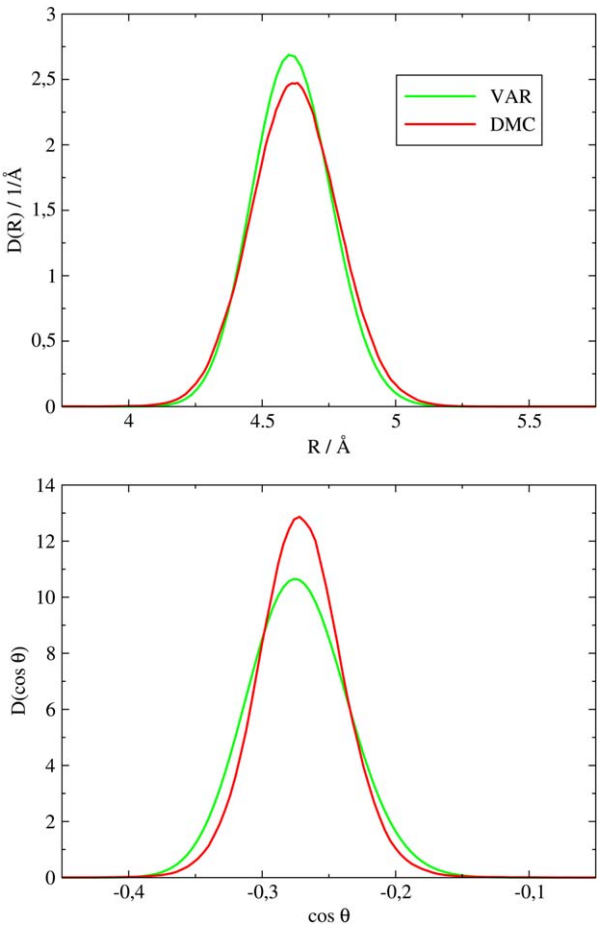

Figure 6. Radial and angular ground-state profiles of the $(X^4\Sigma)$KRb-K complex obtained through the VAR and DMC methods. [Color figure can be viewed in the online issue, which is available at wileyonlinelibrary.com.]

Table 3. Binding energies (E_n, in cm^{-1}) for the ground and lowest six excited states (n) of the ($^4\Sigma$)KRb-K potential calculated through the VAR methodology.

n	E_n
0	−737.818
1	−712.622
2	−708.451
3	−686.248
4	−682.463
5	−679.861
6	−660.306

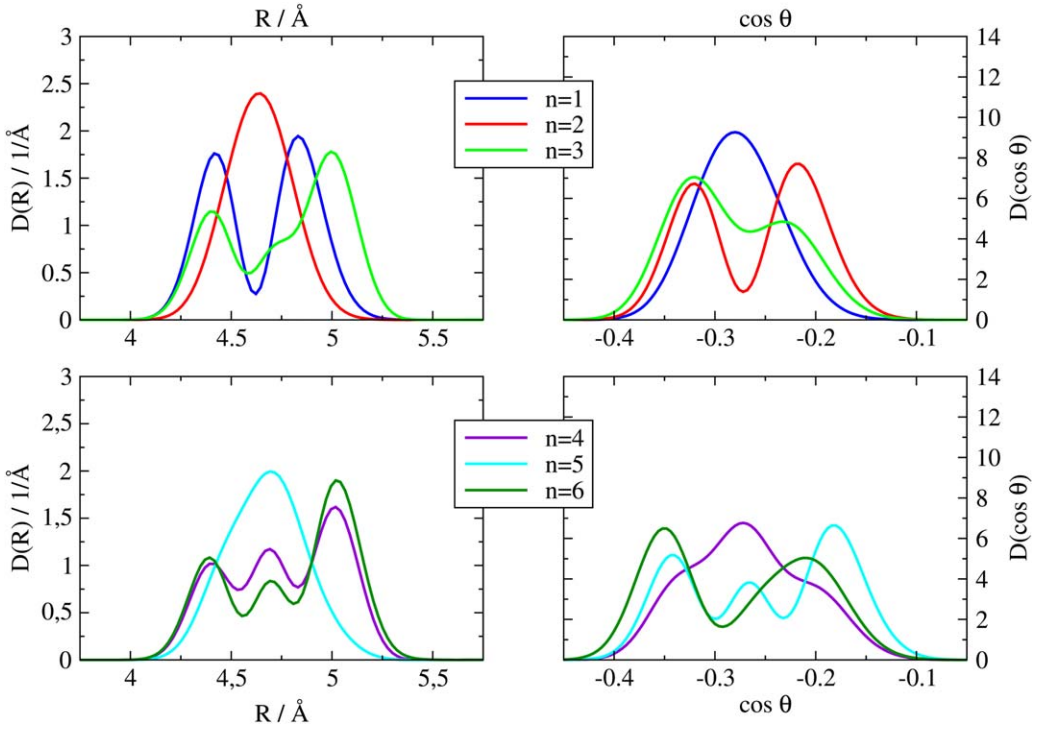

Figure 7. Radial and angular density distributions for the lowest six excited states of the ($X^4\Sigma$)KRb-K complex obtained through the VAR treatment. Upper panels: $n = 1$, 2, and 3; lower panels: $n = 4$, 5, and 6. [Color figure can be viewed in the online issue, which is available at wileyonlinelibrary.com.]

The evolution of the N_w replicas or walkers of the system in the configurational space through the simulation of a diffusion in the imaginary time leads us to the ground-state distribution $f_0 = \Psi_0\Psi_T$. The Green's function is unknown and in the importance sampling DMC framework[68,69] it is splitted into two different contributions, according to the Trotter formula up to first order in $\triangle\tau$:

$$G(\overrightarrow{R}' \leftarrow \overrightarrow{R}, \triangle\tau) \simeq G_d(\overrightarrow{R}' \leftarrow \overrightarrow{R}, \triangle\tau) G_b(\overrightarrow{R}' \leftarrow \overrightarrow{R}, \triangle\tau). \quad (20)$$

G_d, the "diffusional" term, controls the weights of the walkers and G_b, the "branching" term, changes their population.[68] On average, walkers will die in regions where $\Psi_T > \Psi$ and give birth in regions where $\Psi_T < \Psi$. The branching scheme is based on the algorithm presented in various earlier papers.[70,71]

The trial wavefunction of the title system can be expressed as a Gaussian form[72]:

$$\Psi_T(\overrightarrow{R}) = \Psi_{KRb\text{-}K}(\overrightarrow{R}) = e^{-\left\{\left(\frac{x-x_0}{\sqrt{2}\sigma_x}\right)^2 + \left(\frac{y-y_0}{\sqrt{2}\sigma_y}\right)^2\right\}}, \quad (21)$$

in which (x_0, y_0) is the center and (σ_x, σ_y) the spreading of the function.

Numerical Details and Results

Numerical details

Variational treatment. The masses that we have used are (amu): $m_K = 39.0983$ and $m_{Rb} = 85.4678$. A Numerov procedure with 8192 points was used to obtain the radial wavefunctions f_n in the range $1 \leq R \leq 100$, interpolated with 600 Gaussian points to speed up numerical radial quadratures. Sixteen angles in the interval [0,105] were necessary ($N=16$) and $0 \leq j \leq 69$, always with $J = 0$. 101 Gauss-Legendre points in the interval $[0, \pi]$ were considered to expand the dimer-potassium analytical interaction. Parity under inversion is $\epsilon = 1$ and energy was converged to within 10^{-3} cm^{-1}.

Diffusion Monte Carlo technique. We have propagated our stochastic calculations along 5×10^5 steps, as $1 \leq \triangle\tau \leq 500$ hartree^{-1}, a total time of $5\times10^5 - 2.5\times10^8$ hartree^{-1} has been considered, time long enough to ensure convergence in all quantities. The values for the parameters of the trial wavefunction are: $x_0 = -1.25$, $y_0 = 4.45$, and $\sigma_x = \sigma_y = 0.25$. The number of walkers N_w is ranged between 100 and 2500 and for a given fixed value of N_w we have fitted the energy to a simple straight line $E = m\times\triangle\tau + n$, which, therefore, $\rightarrow n$ when $\triangle\tau \rightarrow 0$. In turn the couples (N_w, n) have been extrapolated to the function $n = a + \frac{b}{N_w}$, where a is the parameter of interest because is the energy of the system when $N_w \rightarrow \infty$. The error associated to the value presented corresponds to that of the fitting of a. The DMC geometry distributions belong to the calculations with $N_w = 2500$ and $\triangle\tau = 1$ hartree^{-1}.

Results

In Figure 5 we report the bound-state wavefunctions related to both methods used in this work: VAR and DMC; where a marked sharpness and anisotropy are observed due to the corresponding features of the KRb-K interaction.

The results obtained are in fair agreement with each other and the energies for the ground vibrational state are (cm^{-1}): E(VAR)=–737.818 and E(DMC)= -737.80 ± 0.24. The VAR value is slightly deeper than the DMC one and within its error bar. The small ZPE ($\sim$30 cm^{-1}, about 4% of the total deep well) indicates that the system relative masses of the partners play a significant role in increasing quantum localization of the complex, although quantum effects are still deemed to be important; as an example of this importance 628 bound states are found in the VAR method. In Figure 6, radial and angular profiles corresponding to VAR and DMC computed ground vibrational states are shown, with both curves peaking at the same value of R and cos θ: $R_{mx} \sim 4.6$ Å, $(\cos\theta)_{mx} = -0.26 \Rightarrow \theta_{mx} \sim 105^{\circ}$ (i.e., the well of the PES).

As already mentioned above, we have also computed all the excited states provided by the VAR treatment, Table 3 and Figure 7. The largest/smallest differences in energy between two neighboring states are due to radial/angular excitations: $n = 1,3$, and 6 in the former case, $n = 2$ and 5 in the latter, with the exception of $n = 4$, which is close in energy but radially excited with respect to $n = 3$. The general trend for the vibrationally excited states is seen to explore different regions of the space, although always nearby the minimum of the well ($R = 4.60$ Å, $\theta = 105^{\circ}$): $4.25 \lesssim R \lesssim 5.25, 100^{\circ} \lesssim \theta \lesssim 109^{\circ}$.

Conclusions

We have presented in this work a high level *ab initio* computed PES of the complex ($X^4\Sigma$)KRb-K with the dimer at its lowest triplet $^3\Sigma$ state and fixed to the equilibrium distance, for which the calculations have been carried out with the MOLPRO 2006.1 package. The ECPs and the basis set for K/Rb have been ECP10MDF/ECP28MDF, respectively, as discussed earlier.

The main conclusions we have reached here are the following:

1. The PES is very anisotropic, with one minimum which identifies a T-type geometry for the complex. Its minimum is placed at R=4.60 Å and $\theta = 105^{\circ}$, with a well depth of 767.7 cm^{-1}.
2. The ground-state vibrational level for the complex turns out to be strongly bound, with an energy of ~ -737.8 cm^{-1}. The maxima of the density distribution is found to be at $R \sim 4.6$ Å and $\theta \sim 105^{\circ}$, situated above the minimum of the PES. The VAR and DMC methods agree fairly well in providing the energetics and the geometry description of the complex.
3. The VAR procedure reveals a large number of bound excited states of the aggregate and some of the excited states reported here clearly reveal both radial and angular excited modes.

The surface presented in this work makes it possible to further carry out additional studies which can deal with elastic and inelastic scattering processes involving K+KRb, possibly followed later on by an equivalent study on the ($X^2\Sigma$)KRb-K complex. Our results aim at contributing to the understanding of physical aspects at the molecular level for the special dynamical regimes of ultracold molecules and provide valuable information already relevant for guiding the search for future developments.[73,74]

Acknowledgments

The calculations have been done in the Centro de Cálculo (CSIC), to whom the authors are grateful. The aid of COST Action CM1002 (CODECS) is also appreciated.

Keywords: *ab initio* calculations · electronic structure · bound states · variational methodology · diffusion monte carlo

How to cite this article: D. López-Durán, N. F. Aguirre, G. Delgado-Barrio, P. Villarreal, F. A. Gianturco, M. P. Lara-Castells. *Int. J. Quantum Chem.* **2014**, DOI: 10.1002/qua.24759

[1] J. J. Hudson, B. E. Sauer, M. R. Tarbutt, E. A. Hinds, *Phys. Rev. Lett.* **2002**, *89*, 023003.
[2] L. B. Heindrick, W. Ubachs, *Faraday Discuss.* **2009**, *142*, 25.
[3] D. DeMille, *Phys. Rev. Lett.* **2002**, *88*, 067901.
[4] M. T. Bell, T. P. Softley, *Mol. Phys.* **2009**, *107*, 99.
[5] M. A. Baranov, *Phys. Rep.* **2008**, *464*, 71.
[6] G. Pupillo, A. Micheli, H. P. Buchler, P. Zoller, Cold Molecules: Theory, Experiments, Applications; CRC Press: Boca Raton, **2009**.
[7] C. Ospelkaus, S. Ospelkaus, L. Humbert, P. Ernst, K. Sengstock, K. Bongs, *Phys. Rev. Lett.* **2006**, *97*, 120402.
[8] F. Ferlaino, C. D'Errico, G. Roati, M. Zaccanti, M. Inguscio, G. Modugno, *Phys. Rev. A* **2006**, *73*, 040702.
[9] C. Klempt, T. Henninger, O. Topic, J. Will, W. Ertmer, E. Tiemann, J. Arlt, *Phys. Rev. A* **2007**, *76*, 020701.
[10] C. Weber, G. Barontini, J. Catani, G. Thalhammer, M. Inguscio, F. Minardi, *Phys. Rev. A* **2008**, *78*, 061601.
[11] J. J. Zirbel, K.-K. Ni, S. Ospelkaus, J. P. D'Incao, C. E. Wieman, J. Ye, D. S. Jin, *Phys. Rev. Lett.* **2008**, *100*, 143201.
[12] J. J. Zirbel, K.-K. Ni, S. Ospelkaus, T. L. Nicholson, M. L. Olsen, P. S. Julienne, C. E. Wieman, J. Ye, D. S. Jin, *Phys. Rev. A* **2008**, *78*, 013416.
[13] N. V. Vitanov, M. Fleischhauer, B. W. Shore, K. Bergmann, *Adv. At. Mol. Opt. Phys.* **2001**, *46*, 55.
[14] K. Bergmann, H. Theuer, B. W. Shore, *Rev. Mod. Phys.* **1998**, *70*, 1003.
[15] J. G. Danzl, E. Haller, M. Gustavsson, M. J. Mark, R. Hart, N. Boulufa, O. Dulieu, H. Ritsch, H. C. Nägerl, *Science* **2008**, *321*, 1062.
[16] K.-K. Ni, S. Ospelkaus, M. H. G. de Miranda, A. Pe'er, B. Neyenhuis, J. J. Zirbel, S. Kotochigova, P. S. Julienne, D. S. Jin, J. Ye, *Science* **2008**, *322*, 231.
[17] F. Lang, K. Winkler, C. Strauss, R. Grimm, J. H. Denschlag, *Phys. Rev. Lett.* **2008**, *101*, 133005.
[18] J. G. Danzl, M. J. Mark, E. Haller, M. Gustavsson, R. Hart, J. Aldegunde, J. M. Hutson, H.-C. Nägerl, *Nat. Phys.* **2010**, *6*, 265.
[19] S. Ospelkaus, K.-K. Ni, M. H. G. de Miranda, B. Neyenhuis, D. Wang, S. Kotochigova, P. S. Julienne, D. S. Jin, and J. Ye, *Faraday Discuss.* **2009**, *142*, 351.
[20] S. Ospelkaus, K.-K. Ni, G. Quéméner, B. Neyenhuis, D. Wang, M. H. G. de Miranda, J. L. Bohn, J. Ye, D. S. Jin, *Phys. Rev. Lett.* **2010**, *104*, 030402.
[21] S. Ospelkaus, K.-K. Ni, D. Wang, M. H. G. de Miranda, B. Neyenhuis, G. Quéméner, P. S. Julienne, J. L. Bohn, D. S. Jin, J. Ye, *Science* **2010**, *327*, 853.
[22] K. K. Ni, S. Ospelkaus, D. Wang, G. Quéméner, B. Neyenhuis, M. H. G. de Miranda J. L. Bohn, J. Ye, D. S. Jin, *Nature* **2010**, *464*, 1324.
[23] M. H. G. de Miranda, A. Chotia, B. Neyenhuis, D. Wang, G. Quéméner, S. Ospelkaus, J. L. Bohn, J. Ye, D. S. Jin, *Nat. Phys.* **2011**, *7*, 502.

[24] B. Neyenhuis, B. Yan, S. A. Moses, J. P. Covey, A. Chotia, A. Petrov, S. Kotochigova, J. Ye, D. S. Jin, *Phys. Rev. Lett.* **2012**, *109*, 230403.
[25] K.-K. Ni, S. Ospelkaus, D. J. Nesbitt, J. Ye, D. S. Jin, *Phys. Chem. Chem. Phys.* **2009**, *11*, 9626.
[26] P. S. Żuchowski, J. M. Hutson, *Phys. Rev. A* **2010**, *81*, 060703.
[27] J. N. Byrd, J. A. Montgomery, Jr., R. Côté, *Phys. Rev. A* **2010**, *82*, 010502.
[28] J. Higgins, T. Hollebeek, J. Reho, T.-S. Ho, K. K. Lehmann, H. Rabitz, G. Scoles, *J. Chem. Phys.* **2000**, *112*, 5751.
[29] G. Quéméner, P. Honvault, J.-M. Launay, *Phys. Rev. A* **2005**, *71*, 032722.
[30] M. T. Cvitaš, P. Soldán, J. M. Hutson, P. Honvault, J.-M. Launay, *J. Chem. Phys.* **2007**, *127*, 074302.
[31] J. Higgins, W. E. Ernst, C. Callegari, J. Reho, K. K. Lehmann, G. Scoles, M. Gutowski, *Phys. Rev. Lett.* **1996**, *77*, 4532.
[32] N. J. Wright, J. M. Hutson, *J. Chem. Phys.* **1999**, *112*, 3214.
[33] M. T. Cvitaš, P. Soldán, J. M. Hutson, P. Honvault, J.-M. Launay, *Phys. Rev. Lett.* **2005**, *94*, 033201.
[34] P. Soldán, M. T. Cvitaš, J. M. Hutson, P. Honvault, J.-M. Launay, *Phys. Rev. Lett.* **2005**, *89*, 153201.
[35] H. Cybulski, R. V. Krems, H. R. Sadeghpour, A. Dalgarno, J. Kłos, G. C. Groenenboom, A. van der Avoird, D. Zgid, G. Chałasiński, *J. Chem. Phys.* **2005**, *122*, 094307.
[36] B. C. Shepler, B. H. Yang, T. J. D. Kumar, P. C. Stancil, J. M. Bowman, N. Balakrishnan, P. Zhang, E. Bodo, A. Dalgarno, *Astron. Astrophys.* **2007**, *475*, L15.
[37] H.-J. Werner, P. J. Knowles, R. Lindh, F. R. Manby, M. Schütz, P. Celani, T. Korona, G. Rauhut, R. D. Amos, A. Bernhardsson, A. Berning, D. L. Cooper, M. J. O. Deegan, A. J. Dobbyn, F. Eckert, C. Hampel, G. Hetzer, A. W. Lloyd, S. J. McNicholas, W. Meyer, M. E. Mura, A. Nicklass, P. Palmieri, R. Pitzer, U. Schumann, H. Stoll, A. J. Stone, R. Tarroni, T. Thorsteinsson, Molpro, Version 2006.1, A Package of Ab Initio Programs, 2006. Available at: http://www.molpro.net. Accessed on 31 August, 2014.
[38] S. F. Boys, F. Bernardi, *Mol. Phys.* **1970**, *19*, 553.
[39] I. S. Lim, P. Schwerdtfeger, B. Metz, H. Stoll, *J. Chem. Phys.* **2005**, *122*, 104103.
[40] F. Weigend, R. Ahlrichs, *Phys. Chem. Chem. Phys.* **2005**, *7*, 3297.
[41] A. Pashov, O. Docenko, M. Tamanis, R. Ferber, H. Knöckel, E. Tieman, *Phys. Rev. A* **2007**, *76*, 022511.
[42] S. Rousseau, A. R. Allouche, M. Aubert-Frécon, *J. Mol. Spectrosc.* **2000**, *203*, 235.
[43] S. J. Park, Y. J. Choi, Y. S. Lee, G.-H. Jeung, *Chem. Phys.* **2000**, *257*, 135.
[44] S. Kotochigova, P. S. Julienne, E. Tiesinga, *Phys. Rev. A* **2003**, *68*, 022501.
[45] P. Soldán, V. Špirko, *J. Chem. Phys.* **2007**, *127*, 121101.
[46] P. Soldán, *Phys. Rev. A* **2010**, *82*, 034701.
[47] W. T. Zemke, R. Côté, C. Stwalley, *Phys. Rev. A* **2005**, *71*, 062706.
[48] M. Grüning, O. V. Gritsenko, S. V. A. van Gisbergen, E. J. Baerends, *J. Chem. Phys.* **2001**, *114*, 652.
[49] A. Derevianko, W. R. Johnson, M. S. Safranova, J. F. Babb, *Phys. Rev. Lett.* **1999**, *82*, 3589.
[50] S. G. Porsev, D. Derevianko, *J. Chem. Phys.* **2003**, *119*, 844.
[51] A. Derevianko, J. F. Babb, A. Dalgarno, *Phys. Rev. A* **2001**, *63*, 052704.
[52] J. A. Beswick, G. Delgado-Barrio, *J. Chem. Phys.* **1980**, *73*, 3653.
[53] F. A. Gianturco, The Transfer of Molecular Energy by Collisions; Springer: Berlin, **1979**.
[54] G. Auböck, J. Nagl, C. Callegari, W. E. Ernst, *J. Phys. Chem. A* **2007**, *111*, 7404.
[55] H. Lefebvre-Brion, R. W. Field, Perturbations in the Spectra of Diatomic Molecules; Academic Press, Inc.: Orlando, FL, **1986**.
[56] V. Aquilanti, S. Cavalli, G. Grossi, *Z. Phys. D* **1996**, *36*, 215.
[57] O. Roncero, M. P. de Lara-Castells, G. Delgado-Barrio, P. Villarreal, T. Stoecklin, A. Voronin, J. C. Rayez, *J. Chem. Phys.* **2008**, *128*, 164313.
[58] D. Secrest, W. Eastes, *J. Chem. Phys.* **1972**, *56*, 2502.
[59] Linear Algebra Package 3.2.1, 2009. Available at: http://www.netlib.org/lapack. Accessed on 31 August, 2014.
[60] Intel MKL 10.2, 2009. Available at: http: //software.intel.com/en-us/intel-mkl/. Accessed on 31 August, 2014.
[61] C. Di Paola, F. A. Gianturco, D. López-Durán, M. P. de Lara-Castells, G. Delgado-Barrio, P. Villarreal, J. Jellinek, *Chem. Phys. Chem.* **2005**, *6*, 1348.
[62] D. M. Ceperley, B. Adler, *Science* **1986**, *231*, 555.
[63] W. A. Lester, Jr., B. L. Hammond, *Annu. Rev. Phys. Chem.* **1990**, *41*, 283.
[64] R. N. Barnett, P. J. Reynolds, *J. Comput. Phys.* **1991**, *96*, 258.
[65] M. Lewerenz, R. O. Watts, *Mol. Phys.* **1994**, *81*, 1075.
[66] J. B. Anderson, *Int. Rev. Phys. Chem.* **1995**, *14*, 85.
[67] M. Lewerenz, *J. Chem. Phys.* **1996**, *104*, 1028.
[68] L. B. Hammond, W. A. Lester, Jr., P. J. Reynolds, Monte Carlo Methods in Ab Initio Quantum Chemistry; World Scientific: Singapore, **1994**.
[69] P. J. Reynolds, D. M. Ceperley, B. J. Alder, W. A. Lester, Jr., *J. Chem. Phys.* **1982**, *77*, 5593.
[70] F. Paesani, F. A. Gianturco, *J. Chem. Phys.* **2002**, *116*, 10170.
[71] F. Paesani, F. A. Gianturco, *J. Chem. Phys.* **2002**, *117*, 709.
[72] E. Bodo, E. Coccia, D. López-Durán, F. A. Gianturco, *Phys. Scr.* **2007**, *76*, C104.
[73] J. F. E. Croft, A. O. G. Wallis, J. M. Hutson, *Phys. Rev. A* **2011**, *84*, 042703.
[74] J. F. E. Croft, J. M. Hutson, P. S. Julienne, *Phys. Rev. A* **2012**, *86*, 022711.

Received: 20 June 2014
Revised: 7 August 2014
Accepted: 12 August 2014
Published online on Wiley Online Library